crystals

MDPI

Article

Effect of Fungal Metabolism on Zn Minerals Formation: The Case of *Aspergillus niger* and *Penicillium chrysogenum*

Katerina V. Sazanova [1,2,*], Marina S. Zelenskaya [3], Anatoliy V. Korneev [4,5], Elena V. Bakhvalova [5], Dmitry Yu. Vlasov [1,3] and Olga V. Frank-Kamenetskaya [4]

1 Komarov Botanical Research Institute of Russian Academy of Science, Prof. Popov Street 2, 197376 Saint Petersburg, Russia; d.vlasov@spbu.ru
2 Archive of the Russian Academy of Sciences, St. Petersburg Branch, Kievskaya Street 5, 196084 Saint Petersburg, Russia
3 Department of Botany, Saint Petersburg State University, University emb. 7/9, 199034 Saint Petersburg, Russia; m.zelenskaya@spbu.ru
4 Department of Crystallography, Saint Petersburg State University, University emb. 7/9, 199034 Saint Petersburg, Russia; 282520@mail.ru (A.V.K.); o.frank-kamenetskaia@spbu.ru (O.V.F.-K.)
5 "ECROSKHIM" Ltd., Koli Tomchaka Street 25, lit. ZH, 19600 Saint Petersburg, Russia; bakhvalova@ecohim.ru
* Correspondence: ksazanova@binran.ru

Abstract: Soil fungi are significantly resistant to heavy metals, which allows them to be used in biotechnologies for environmental bioremediation. In order to clarify the prospects for using the fungi in Zn-detoxifying technologies, we investigated in vitro the effect of fungal metabolism on Zn minerals formation. The cultivation of fungi with different acid-producing activities (*Aspergillus niger* and *Penicillium chrysogenum*) was carried out in a liquid Czapek–Dox nutrient medium with Zn concentrations from 250 to 2000 µmol within 28 days. The quantitates of low-molecular-weight organic acids, phosphates, and hydrophosphates ions in the medium were determined through chromatography–mass spectrometry; analysis of biomineralization products was carried out through powder X-ray diffraction, scanning electron microscopy, and energy-dispersive X-ray spectroscopy. It was found that Zn in concentrations 250–500 µmol acts as a physiologically essential element, activating the growth of fungal mycelium, while at high concentrations (1000–2000 µmol), Zn acts as a toxic heavy metal, inhibiting fungal growth. Zn also activates the formation of oxalic acid by both species of fungi. But *A. niger* strongly acidified the medium, while *P. chrysogenum* leaves the medium pH close to neutral or slightly alkaline. Oxalate and phosphate crystallization occur with the participation of both fungal species. The ratio of biogenic oxalates and phosphates is directly dependent on the acid-reducing capacity of fungi. The solid solutions of katsarosite–glushinskite of the isodimorphic series with the general formula $(Zn,Mg)C_2O_4 \cdot 2H_2O$ (Mg ions comes from Czapek–Dox medium) were detected at all Zn concentrations in a wide range of pH (from 2 to 9.0). The transition from monoclinic (α-modifications) to orthorhombic (β-modifications) occurs at the ratio Mg/Zn > 1. Fungal zinc phosphate hopeite $Zn_3(PO_4)_2 \cdot 4H_2O$ was formed at a near-neutral pH at high Zn concentrations (1000 and 2000 µmol/L). In the Zn example, it was shown that not only oxalate but also phosphate fungal biomineralization can be used for the environment detoxification of heavy metals. The application of phosphate biomineralization seems promising in the case of severe pollutions. To create a near-neutral medium favorable for the formation of phosphates, it is advisable to use soil fungi non-producing or weakly producing organic acids (for example, *P. chrysogenum*).

Keywords: microbial biomineralization; fungal metabolism; *Aspergillus niger*; *Penicillium chrysogenum*; zinc; katsarosite; hopeite; bioremediation

Academic Editor: Ruikang Tang

Received: 31 December 2024
Revised: 19 January 2025
Accepted: 21 January 2025
Published: 23 January 2025

Citation: Sazanova, K.V.; Zelenskaya, M.S.; Korneev, A.V.; Bakhvalova, E.V.; Vlasov, D.Y.; Frank-Kamenetskaya, O.V. Effect of Fungal Metabolism on Zn Minerals Formation: The Case of *Aspergillus niger* and *Penicillium chrysogenum*. *Crystals* **2025**, *15*, 118. https://doi.org/10.3390/cryst15020118

1. Introduction

Soil fungi are significantly resistant to heavy metals, allowing them to survive in environments with high concentrations of toxic elements [1–3]. There are numerous studies for the use of fungi in environmental bioremediation technology [4–13]. Temporary changes in the bioavailability of metals by fungi may be due to the sorption of metals on the fungal cell walls. The presence of extracellular polymeric compounds produced by fungi in the medium greatly increases the intensity of metal sorption [1–3,14]. However, over time, the adsorbed metals are released back into the environment [14]. A more long-term mechanism of metal immobilization by fungi is due to their ability to precipitate metals in the form of insoluble or low-soluble crystalline phases (biomineralizaion), mostly oxalates [15–20].

Another promising approach to reducing toxicity and immobilization of metals is to precipitate low-soluble metal phosphates by adding phosphorus compounds to polluted soil [21–24]. Phosphorus (P) homeostasis is an integral part of fungal metabolism, their adaptations, and a key mediator in antagonistic relationships between fungi and other organisms. There are many studies demonstrating the role of fungi in the dissolution of poorly soluble metal phosphates, including zinc phosphate [25], tricalcium phosphate [26], and ammonium magnesium phosphate struvite [27,28]. The organic acids secretion by fungi leads to the release of P from low-soluble phosphates and an increase in P bioavailability [27,28]. The ability of fungi to increase P bioavailability is exploited by plants that form mycorrhiza [29].

There is very little data about the formation of phosphates under the influence of fungi, although interest in phosphate biomineralization has appeared in the scientific world in recent years. First of all, this is due to the possibility of using poorly soluble phosphates in biological purification of the environment (wastewater, soils) from organic pollutants [30–32].

Obviously, this process is much larger in scale than is currently known. There are data that hydroxyapatite (calcium phosphate) can be formed in the cytoplasm and on the surface of *Candida albicans* cells [33], chloropyromorphite (lead phosphate) under the influence of the fungi *Paecilomyces javanicus* and *Metarhizium anisopliae* [34,35], uranyl phosphates under the influence of *Aspergillus niger* and *Paecilomyces javanicus* [36], and struvite (magnesium ammonium phosphate hexahydrate—($MgNH_4PO_4 \cdot 6H_2O$) under the influence of *Penicillium chrysogenum* [37].

Zinc (Zn) is one of the most common heavy metals in the Earth's crust. In soils, Zn is generally distributed unevenly, and its content ranges from 10 to 300 mg/kg. Zn values above 150 mg/kg^{-1} are considered high and potentially toxic [38]. The concentration of Zn in nature, like many other potentially toxic elements (As, Ba, Cd, Cr, Cu, Ni, Pb, Co, Se) increases greatly as a result of technogenic pollution [12,38–42]. The main anthropogenic sources of Zn are related to the non-ferric metal industry and agricultural practice. High levels of soil Zn pollution are found in the vicinity of industrial metallurgical enterprises, for example, in the Dhaka Export Processing Zone, Bangladesh [41] and in some places in the Orenburg region, Russia [42].

Zn is essential for living organisms, as it participates in many important metabolic processes and is a cofactor for many enzymes. However, at high concentrations, Zn is dangerous for animals, plants, fungi, and microorganisms. Excessive Zn content in the soil can not only directly affect the physiological properties of plants but also disrupt the transport of other elements in the plant root and thereby cause their deficiency [43].

The Zn toxicity for organisms is determined not only by its concentration but also by the bioavailability of the element, which in turn depends significantly on the metabolic processes of the soil biota [1–3,44]. Thus, the development of biotechnologies for Zn immobilization using fungal biomineralization is a very important task, for the solution of

which it is necessary to study the influence of metabolism of various types of fungi on Zn minerals formation.

Zinc oxalate (biomineral katsarosite) $Zn(C_2O_4)\cdot 2H_2O$ formed under the action of fungi and lichens that produce oxalic acid [18,45–47] belongs to a family of natural (humboldtine group) oxalates with the general formula $Me^{2+}(C_2O_4)\cdot 2H_2O$ (Me = Fe, Mn, Mg, Zn, Ni, Co) [48]. The humboldtine group, besides katsarosite, includes the following isotypical minerals: humboldtine (Fe), lindbergite (Mn), glushinskite (Mg), and andreybulahite (Ni) [47,49–52]. In nature, these minerals are often found in the form of solid solutions [29]. For a long time, all minerals of humboldtine group were considered monoclinic (sp. gr. *C2/c*). It was later shown that they can exist in the monoclinic (sp. gr. *C2/c*) and orthorhombic (*Cccm* or *Fddd*) polymorphic modifications [51,52]. Monoclinic *C2/c* structures belong to α-modification; orthorhombic *Fddd* and *Cccm* are both β-modifications.

Previously, we have shown that zinc phosphate hopeite can be formed under the activity of the fungus *Penicillium chrysogenum* in a Zn-containing medium [53]. Zinc phosphate tetrahydrate hopeite $Zn_3(PO_4)_2\cdot 4H_2O$ (sp. gr. *Pnma*) is the most stable zinc phosphate that can be formed with the participation of fungi [21,24]. These are two known varieties of hopeite, α-hopeite and β-hopeite, which differ slightly in their optical properties and thermal behavior. These two varieties differ in the orientation of one water molecule in the crystal structure [54]. In acidic conditions, hopeite is replaced by tarbuttite $Zn_2(PO_4)(OH)$. Hopeite, like some other metal phosphates, has low solubility (Ksp = 10–35.5), indicating its potential for soil restoration [21]. However, biotechnologies for soil bioremediation based on the use of hopeite and other phosphates have not yet been developed. The prospects for creating technologies using hopeite are confirmed by the fact that hopeite is a thermodynamically stable mineral, thus controlling the mobility of Zn in polluted soils [24]. However, there is evidence that hopeite in agricultural soils can influence plant nutrition of Zn and P, being a slowly soluble reservoir of these elements [40]. P availability in soils worldwide is generally low. Most soils are deficient in available P; unless fertilized, they will not meet plant phosphorus requirements [55]. Thus, under the effect of various types of fungi in a medium containing Zn, crystallization of both oxalates and phosphates can occur. Earlier, using the example of *Aspergillus niger* and *P. chrysogenum*, we showed that the phase formation happening with their participation the phase formation depends on the acid-forming activity of the fungi [53].

In order to study the patterns of Zn mineral formation under the influence of fungi and to conclude the prospects for using the fungi for Zn-detoxifying biotechnologies, it is necessary to identify the effect of Zn concentration on the growth and metabolism of fungi with different acid producing activity and to clarify how these patterns affect the biomineralization processes.

2. Materials and Methods

2.1. Fungal Strains and Experimental Conditions

Two strains of fungi (*Aspergillus niger* and *Penicillium chrysogenum*) were selected for this study, as we have shown previously [18,19,37,56,57], which differ greatly in the production of organic acids. *A. niger* produces significantly more organic acids, including oxalic acid, and thus acidifies the nutrient medium, while *P. chrysogenum* has urease activity, which leads to alkalization of the nutrient medium.

A. niger strain Ch4/07 (Genbank accession number KF768341) was isolated from a damaged marble surface (Chersonesos Taurica Museum-Reserve, Sevastopol, Crimea). *P. chrysogenum* strain Cs/21 (Genbank accession number OP758843) was isolated from surface deposits on the bronze sculpture of Farnese Hercules (TsarskoyeSelo State Museum-

Reserve). *P. chrysogenum* and *A. niger* are the most common soil fungus, also found on many other substrates, including subaerial biofilms on rock surfaces.

The fungi were cultivated using a surface method in cultivation mattresses on the liquid Czapek–Dox nutrient medium (g/L: glucose—30; $NaNO_3$-2.0; KH_2PO_4-1.0; $MgSO_4 \cdot 7H_2O$-0.5; KCl-0.5; $FeSO_4 \cdot 7H_2O$-0.01). The initial pH of the medium was 6.0. Zn was added to the crystallization medium (volume 30 mL) as $ZnSO_4 \cdot 7H_2O$ in the following concentrations: 0 μmol/L, 250 μmol/L (0.07 g/L), 500 μmol/L (0.14 g/L), 1000 μmol/L (0.29 g/L), and 2000 μmol/L (0.58). In order to distinguish the influence of the nutrient medium components and fungal metabolites on the phase composition of the crystallization products, additional syntheses at all zinc concentrations without the fungi were carried out. All the experiments were carried out in triplicate at 25 °C, within 28 days.

2.2. Research Methods

During the experiment, the amount of mycelium biomass was monitored via a gravimetric method, and the pH of the cultural liquid was measured (pH meter Checker 1, HI98103) every 7 days. The concentration of free Zn in the medium after the chemical hopeite precipitation was determined using an X-ray fluorescent (XRF) analysis. The composition of low-molecular-weight organic acids and phosphate concentration in the fungal cultural liquid were determined via gas chromatography–mass spectrometry (GC-MS) on the fourteenth and twenty-eighth days. The phase composition of crystallization products was determined using X-ray diffraction (PXRD). Additionally, light and scanning electron microscopy (SEM) with chemical composition control by energy-dispersive X-ray spectroscopy (EDX) were used. This allowed for phases present in very small quantities (beyond the sensitivity of PXRD) to be identified. In addition, the morphology of the formed crystals and their intergrowths was studied, which allowed for reconstructing the conditions of their formation to reconstruct.

Light microscopy and SEM were carried out on days 7, 14, 21, and 28 of the experiment. PXRD was performed on day 28 for both fungal species at all Zn concentrations and on days 7–21 selectively, depending on light microscopy and SEM data. To analyze the crystallization products, the mycelium of the fungi with crystals was used.

2.2.1. Gas Chromatography–Mass Spectrometry (GC-MS)

Sample preparation

Organic acids, hydrophosphate ions (H_2PO^{4-}, $HPO_4{}^{2-}$), and phosphate ions ($PO_4{}^{-}$) in the cultural liquid were analyzed as their total concentration (in the form of soluble salts and water-insoluble salts) as well as the soluble form separately. Then, the amount of organic acids, hydrophosphate ions (H_2PO^{4-}, $HPO_4{}^{2-}$), and phosphate ions ($PO_4{}^{-}$) in the insoluble form was calculated as the difference in the total concentration and the concentration of acids in the soluble form. To analyze the total acids concentration, an aliquot of cultural liquid (10 mL) was treated with 1N HCl and passed through a cation exchanger (KU-2-8). To determine free acids and their soluble salts, a native aliquot (10 mL), without HCl treatment, of the culture liquid was passed through a cation exchanger (KU-2-8). The resulting solutions of organic acids were dried on a rotary evaporator at 40 °C. The dried residue were dissolved in pyridine (50 μL) and derivatized with BSTFA (N,O-bis-3-methylsilyl-3-F-acetamide) (50 μL) at 100 °C for 15 min.

GC-MS analysis

Derivatized samples were analyzed on a Maestro instrument (Interlab, Moscow, Russia) with an Agilent 5975 mass-selective detector (Santa Clara, CA, USA). An HP-5MS column 30 m × 0.25 mm × 0.25 μm was used. The obtained chromatograms were recorded by the total ion current. Then, the mass spectrometric information was processed and

interpreted using an AMDIS program (http://www.amdis.net/index.html, accessed on 15 November 2024) and the NIST2005 standard library. Quantitative interpretation of the chromatograms by the internal standard method was also carried out using tridecane in the UniChrom program (5.0.19.1180 version) (http://www.unichrom.com/unichrome.shtml, accessed on 20 November 2024).

2.2.2. Light Microscopy

The studies were conducted using microscopes Mikromed 2 (Saint Petersburg, Russia) and Leica with a photo attachment (Wetzlar, Germany).

2.2.3. Scanning Electron Microscopy (SEM) and Energy-Dispersive X-Ray Spectroscopy (EDX)

The investigation was carried out using the TM 3000 (HITACHI, Tokyo, Japan, 2010) microscope. For semiquantitative EDX analysis, the microscope was equipped with the Oxford Inca system (Oxford Instruments, Abingdon, UK), which operated in a low vacuum (60 Pa) mode and at an acceleration voltage of 15 kV. The EDX spectra were analyzed by means of the EDAX Genesis software package.

2.2.4. Powder X-Ray Diffraction (PXRD)

Powder X-ray diffraction (PXRD) patterns were recorded using Miniflex II (Rigaku, Tokyo, Japan) and XRD-9510 (Ecroskhim, Saint Petersburg, Russia) diffractometers using CuKα1 + 2 or CrKα1 + 2 radiation. Samples were ground in mortar and precipitated on a glass holder from ethanol suspension. The measurements were performed in 2ΘCu = 5–60° (2ΘCr = 7.5–100°). Phases were identified using PDF-2 (2020) database. PXRD patterns were also compared with calculated patterns of katsarosite $ZnC_2O_4 \cdot 2H_2O$ [48] and α-hopeite $Zn_3(PO_4)_2 \cdot 4H_2O$ [54] derived from crystal structure data. For convenience, all PXRD patterns were transformed to 2ΘCu scale through Bragg equation.

2.2.5. X-Ray Fluorescent (XRF) Analysis

X-ray fluorescent (XRF) spectra were recorded on a compact XRF spectrometer XRD-9710 PEARL (Ecroskhim, Saint Petersburg, Russia) with a rhodium X-ray tube (25 kV, 10 μA), and the diameter of its primary collimator was 3 mm. A silver filter was used for filtration of primary radiation. The spectrometer was equipped with a semiconductor silicon detector. Liquid samples were placed into sample holders with a bottom of lavsan film. The exposure time was 60 s per sample.

3. Results

3.1. Morphological–Cultural and Physiological–Biochemical Properties of Fungi

3.1.1. The Influence of Zn on the Morphological and Cultural Characteristics of Fungi

On the Zn-free nutrient medium, the mycelium of *A. niger* and *P. chrysogenum* grew fast, a surface mycelial film and sporulation were formed on the fifth to sixth day of the experiment. Zn had a similar general effect on the biomass formation and mycelial morphology for both species of fungi. This effect significantly depended on Zn concentration (Figure 1a,b). At the low concentration (250 and 500 μmol), Zn induced biomass growth of both fungi. The surface mycelial film and sporulation were formed earlier than in the control (on the fourth day). In these cases, like in the Zn-free nutrient medium, growth occurred in two phases: exponential and stationary phase. At concentrations 1000 and 2000 μmol, Zn suppressed the growth and sporulation of both species of fungi. The dynamics of growth had only an exponential phase. The surface film of the mycelium was not formed. At Zn 2000 μmol, the growth began only on the tenth to sixteenth day after spores

inoculation and occurred mainly in the deep form of pellets; the sporulation occurred only at 22–25 days.

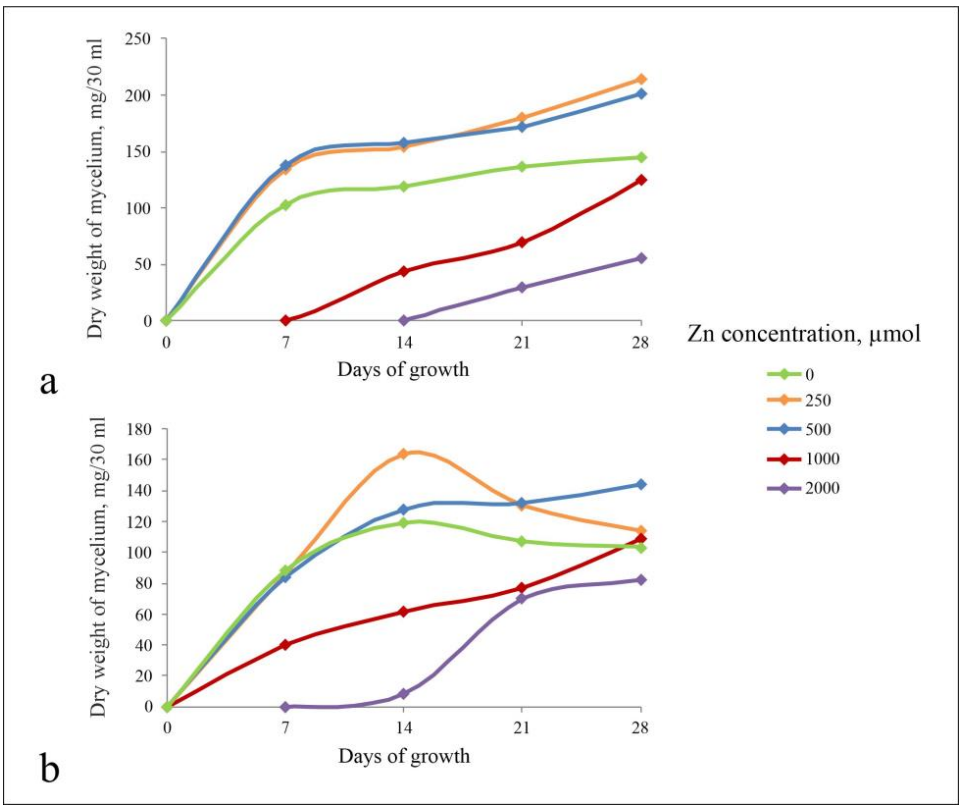

Figure 1. Dynamics of *A. niger* (**a**) and *P. chrysogenum* (**b**) biomass growth at different Zn concentrations.

At Zn concentration 1000 and 2000 µmol, *P. chrysogenum* was more resistant than *A. niger*. The growth dynamics also had two phases: exponential and stationary. Except for Zn-free medium and at the lowest Zn concentrations (250 µmol), the dynamics of *P. chrysogenum* growth had a phase of mycelial lysis for old cultures, which was not observed in the case of *A. niger*.

3.1.2. Metabolism of Fungi at Different Zn Concentrations in the Medium

A. niger acidified the medium at all the Zn concentrations, as well as in the medium without Zn (Figure 2a). The lowest pH values (up to 1.0) were determined in the Zn-free cultural liquid. In the Zn-containing media, the lowest pH values (2.4 and 2.8) were achieved at Zn concentrations of 1000 and 2000 µmol on the twenty-eighth day of the experiment.

P. chrysogenum in all experimental media, except for Zn concentration 2000 µmol, showed a tendency to alkalinize the medium (up to 8.5). Acidification of the medium (less than in *A. niger*, up to pH 4.5 on the fourteenth day) occurred only at the highest Zn concentration (Figure 2b).

Both species of fungi produced low-molecular-weight organic acids (LMWOA): oxalic, citric, malic, succinic, and fumaric. The main acids secreted by the fungi were oxalic and citric (Tables 1 and 2). Succinic, fumaric, and malic acids were present in trace amounts in all cases. The amount of oxalic acid in the cultural liquid of *A. niger* was more than 10 times higher than in the cultural liquid of *P. chrysogenum*. In the cultural liquid of *A. niger*, citric acid in the Zn-free medium prevailed compared to oxalic acid, and vice versa, on Zn-containing media (Table 1).

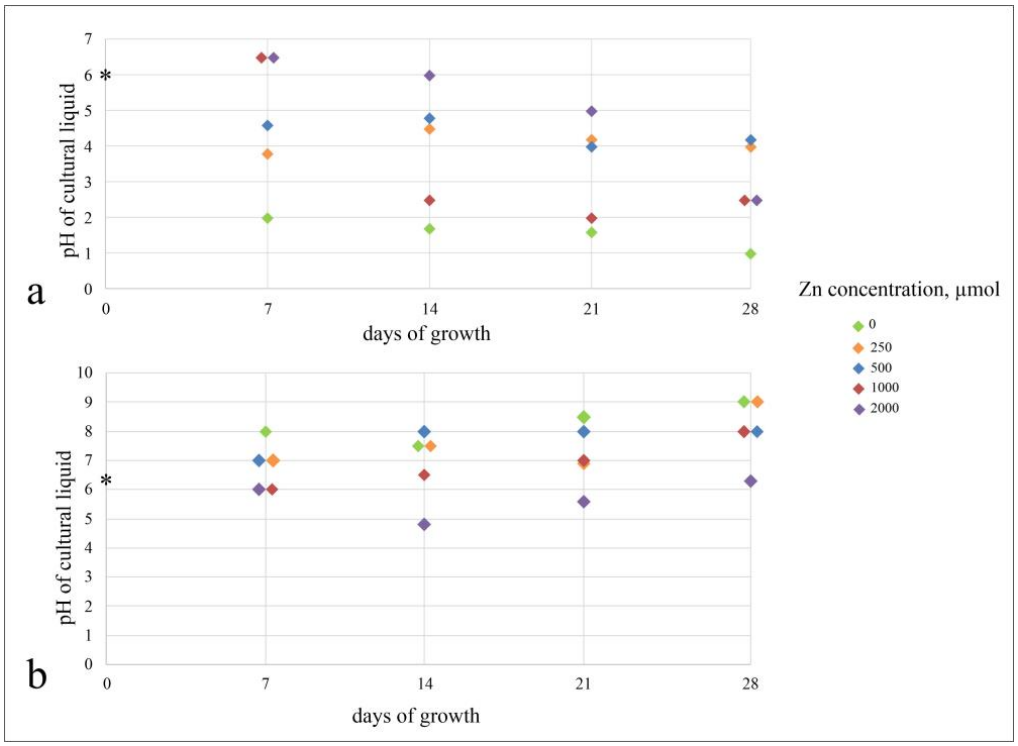

Figure 2. Dynamics of pH value of the cultural liquid under *A. niger* (**a**) and *P. chrysogenum* (**b**) activity at different Zn concentrations. Note: *—initial pH of Czapek–Dox medium.

Table 1. Composition of *A. niger* cultural liquid at different Zn concentrations.

Zn Concentration, µmol		Age of Culture, Days	Organic Acids, µg/mL			$H_2PO_4^-$ + HPO_4^{2-} + PO_4^{3-}, µg/mL		pH
Total	Soluble		Oxalic		Citric	Soluble	Insoluble	
			Soluble	Insoluble	Soluble			
0	0	14	197 ± 20	180 ± 35	280 ± 39	412 ± 93	-	2.8
		28	222 ± 36	257 ± 29	449 ± 39	134 ± 18	-	2.0
250	192	14	127 ± 22	344 ± 43	103 ± 24	375 ± 41	-	4.2
		28	204 ± 25	388 ± 56	57 ± 18	176 ± 22	-	3.9
500	432	14	105 ± 28	480 ± 47	68 ± 16	486 ± 64	-	5.0
		28	110 ± 18	522 ± 28	52 ± 21	212 ± 37	-	5.2
1000	639	14	187 ± 34	640 ± 56	72 ± 11	375 ± 19	-	2.5
		28	255 ± 37	720 ± 66	38 ± 7	176 ± 11	-	2.4
2000	1626	14	-	-	-	540 ± 52	22 ± 8	6.0
		28	302 ± 8	988 ± 88	-	202 ± 64	-	2.8

Oxalic acid produced by *A. niger* was present in the cultural liquid in the form of insoluble salts and soluble form (Table 1). The ratio of free and bound oxalic acid depended on the Zn concentration in the medium: with an increasing Zn concentration, the proportion of oxalate ion bound into insoluble salts increased. In the culture liquid of *P. chrysogenum*, all oxalic acid was in an insoluble form (Table 2).

Table 2. Composition of *P. chysogenum* cultural liquid at different Zn concentrations.

Zn Concentration, μmol		Age of Culture, Days	Organic Acids, μg/mL			$H_2PO_4^-$ + HPO_4^{2-} + PO_4^{3-}, μg/mL		pH
Total	Soluble		Oxalic		Citric	Soluble	Insoluble	
			Soluble	Insoluble	Soluble			
0	0	14	-	38 ± 6	3.1 ± 0.8	304 ± 18	-	8.0
		28	-	64 ± 8	trace	194 ± 16	-	9.0
250	192	14	-	72 ± 11	4.8 ± 0.6	218 ± 18	35 ± 14	7.5
		28	-	86 ± 22	trace	184 ± 12	29 ± 8	9.0
500	432	14	-	104 ± 9	6.4 ± 0.8	222 ± 9	48 ± 14	8.0
		28	-	122 ± 86	5.5 ± 0.8	129 ± 8	37 ± 9	8.0
1000	639	14	-	52 ± 11	4.4 ± 0.7	228 ± 6	56 ± 22	6.5
		28	-	108 ± 22	6.8 ± 0.6	117 ± 4	75 ± 13	8.0
2000	1626	14	-	34 ± 8	4.1 ± 0.4	234 ± 6	74 ± 28	4.8
		28	-	42 ± 13	5.1 ± 0.7	111 ± 4	108 ± 31	6.3

In addition to the acids secreted by the fungi, the cultural liquid contained products of KH_2PO_4 dissociation: hydrophosphate ions ($H_2PO_4^-$, HPO_4^{2-}) and phosphate ions (PO_4^{3-}), which are not chromatographically separable. In the medium without fungi, the concentration of free hydrophosphates and phosphate ions decreases from 695 μg/mL in the control medium to 580 μg/mL as the Zn concentration increases. The total amount of hydrophosphates and phosphate ions in the cultural liquid of fungi decreased with the age of cultures due to P consumption by the mycelium (Tables 2 and 3).

Table 3. Phase composition of crystals formed on *A. niger* mycelium at different Zn concentration formed under the activity of *A. niger.*

Days	Zn Concentration in Solution, μmol							
	250		500		1000		2000	
	Phase Composition	pH	Phase Composition	pH	Phase Composition	pH	Phase Composition	pH
7	Hop (ab), Zn-MgOx (α)	3.8	Hop (ab), Zn-MgOx (α) >> Mg-Kat	4.6	Hop (ab)	6.5	No fungal growth	6.5
14	Zn-MgOx	4.5	Zn-MgOx (α) >> Mg-Kat	4.8	Zn-MgOx (α)~ Mg-Kat	2.5	Hop (ab), **Hop (bio)**	6.0
21		4.2		4.0		2.0	Kat, Hop (ab), **Hop (bio)**	5.0
28	Zn-MgOx (α) >> **Gl (β)**	4.0	Zn-MgOx (α) >> Mg-Kat	4.2		2.5	Kat	2.5

Notes: Hop (ab)—abiogenic hopeite, **Hop (bio)**—biogenic hopeite, Zn-MgOx—Zn-containing Mg-oxalate, Kat—katsarosite, **Gl**—glushinskite, α—monoclinic oxalate modification, β—orthorhombic oxalate modification.

The ratio of water-soluble/-insoluble forms of hydrophosphates and phosphate ions depended on the fungus species. In the cultural liquid of *A. niger,* phosphate was contained in the free form except one case—fourteenth day of growth at Zn concentration 2000 μmol (5% of insoluble hydrophosphates and phosphate ions from the total content).

In the *P. chrysogenum* cultural liquid at all Zn concentrations, the decrease in the hydrophosphates and phosphate ions concentration was associated only with its soluble form, while the insoluble form increased by 10–15%.

As the culture aged, the soluble form of phosphate decreased.

3.2. Phase Formation in the Czapek–Dox Medium at Different Zn Concentrations

3.2.1. Phase Formation in the Absence of Fungi

In the Czapek–Dox nutrient medium (without inoculation of fungal spores), immediately after autoclaving (t = 121 °C, pH = 6.0) at Zn concentrations 250–500 μmol, single needle crystals (up to 500 μm) were found by light and scanning electron microscopy. At Zn concentrations 1000 and 2000 μmol, a precipitate formed numerous large (up to 1.5 mm) needle crystals, sometimes with traces of dissolution (Figure 3a), which were often combined into plates or intergrowths. According to PXRD data, these crystals belong to zinc phosphate tetrahydrate hopeite $Zn_3(PO_4)_2 \cdot 4H_2O$ (Figure 3d) and, according to EDX data, contained an admixture of Mg.

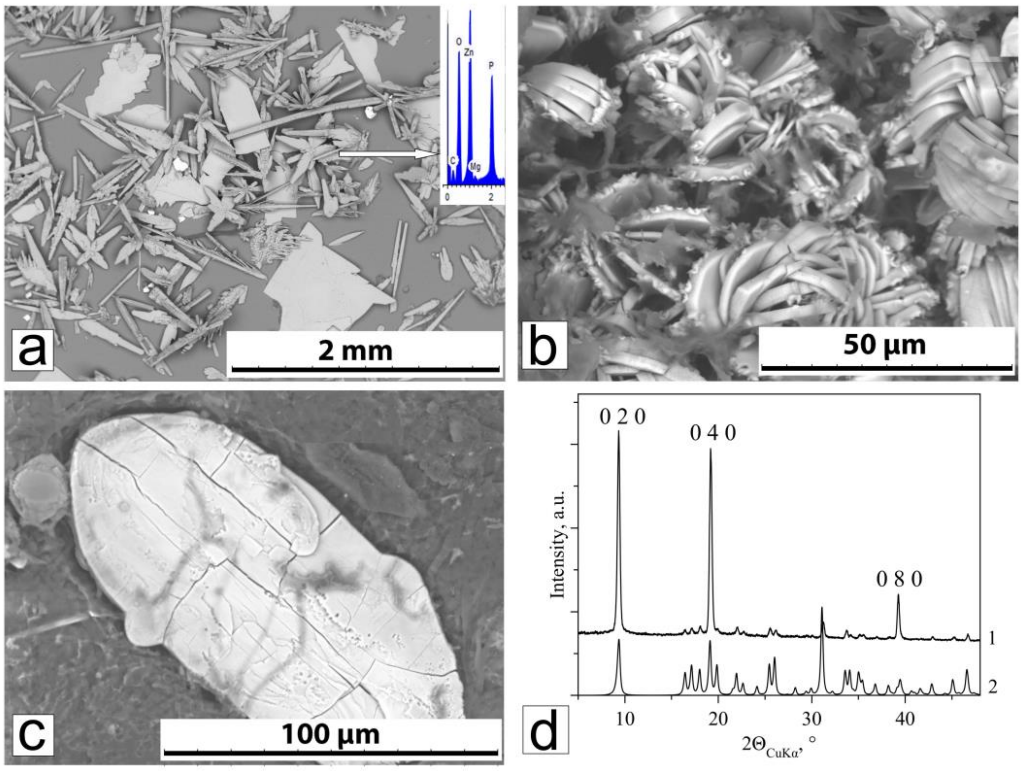

Figure 3. Abiogenic (chemical) hopeite crystals formation in Czapek–Dox medium: (**a**) SEM images of crystals after autoclaving at Zn content 2000 μmol. Inoculation of fungal spores was not performed; (**b**,**c**) SEM images of abiogenic hopeite crystals after cultivation of *P. chrysogenum* at Zn content 1000 μmol; (**d**) PXRD patterns of hopeite crystals on Figure 3a, textured by (010) (1) and calculated from single crystal data (2). The arrow indicates the point on crystals at which the EDX measurement was performed.

The analysis of the concentration of free zinc in solutions (Tables 1 and 2) shows that 64–85% of total Zn remains in the solution in the form of free (bioavailable) Zn, while only 15–36% of the total Zn content is bound in insoluble phosphate.

3.2.2. Phase Composition and Morphology of Crystals Formed Under Action of *A. niger*

In the experiment without Zn, no oxalates and phosphates crystallization occurred on fungal mycelium (Figure 4a). In the region of 2θ Cu = 9.2° (Figure 4a, X phase), a peak is

visible, which is also present in the XRD patterns of Zn-containing crystallization products. It can be assumed that it belongs to the polysaccharide chitosan, which is abundantly present in the cell walls of fungi [58] or a structurally related another organic component of the mycelium.

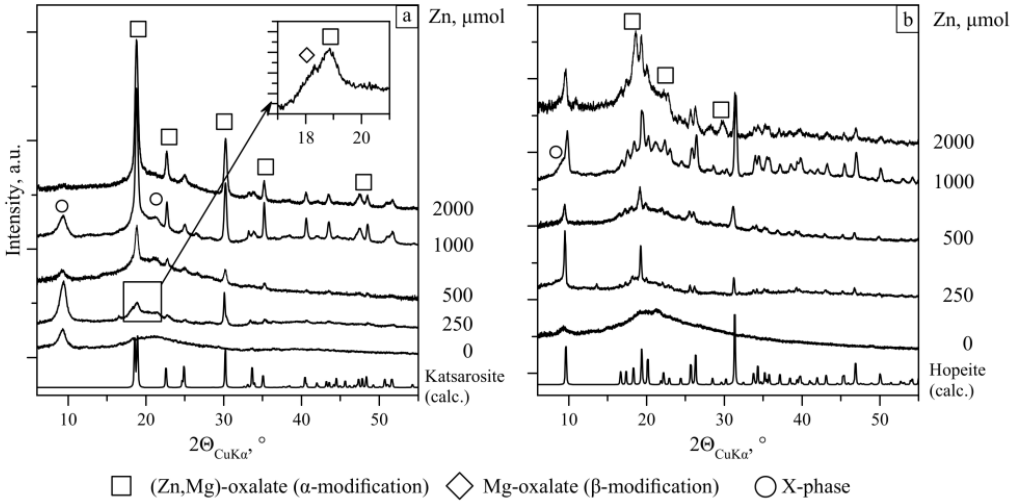

Figure 4. XRD patterns of phases formed under activity of *A. niger* (**a**) and *P. chrysogenum* (**b**). Peaks of hopeite $Zn_3(PO_4)_2 \cdot 4H_2O$ are unsigned.

Metal oxalates formation

In the experiments with Zn concentration 250–2000 μmol in the nutrient medium, according to PXRD, SEM, and EDX data, in the nutrient medium, metal oxalates with the katsarosite structure (monoclinic α-modification) with the general formula (Zn, Mg)$C_2O_4 \cdot 2H_2O$ are formed (Figure 4a, Table 3). At Zn concentration of 250–500 μmol, oxalate crystals appeared on the seventh day, at a Zn concentration of 1000 μmol, crystals appeared on the fourteenth day, and at a Zn concentration of 2000 μmol, crystals appeared on the twenty-first day. With the age of the cultures, their number increased.

As the Zn content in the medium increases, the Mg/Zn ratio in the synthesized oxalates changes. At a Zn concentration of 250 μmol, on the twenty-eighth day of the experiment, magnesium predominates (Mg/Zn ratio = 2.98–1.58), which indicates the formation of magnesium oxalate with different Zn contents. At a Zn content of 250 μmol, on the twenty-eighth day of the experiment, a peak ($2\theta_{Cu}$ = 18.3°) corresponding to the most intense X-ray diffraction reflection of the orthorhombic β-modification (glushinskite mineral) [52] is also identified in the X-ray diffraction patterns (see the inset in Figure 4a.) At a Zn concentration of 500 μmol (Mg/Zn = 1.52–0.32), Mg predominates in 80% of the measured crystals, and Zn predominates in 20%. This suggests that along with the Zn-containing Mg oxalate, which predominates, the mycelium also contains the Mg-containing Zn oxalate katsarosite. At a Zn concentration of 1000 μmol, the range of Mg/Zn ratio interval increases significantly (Mg/Zn = 4.6–0.27). Crystals with a predominance of magnesium (Zn-containing Mg oxalate) and zinc (Mg-containing katsarosite) are present in almost equal quantities. At a Zn concentration of 2000 μmol, magnesium is practically absent (Mg/Zn = 0–0.04). This means that the zinc oxalate katsarosite is present on the mycelium only.

It can be clearly seen that at a Zn concentration of 250 μmol, a number of intergrowths of plate oxalate crystals were observed, located relative to each other at an angle close to 90 degrees (Figure 5a). The sizes of intergrowths reached 80 μm. At a Zn concentration of 500 μmol, the number of intergrowths increased, as well as their size (150–250 μm) (Figure 5b). At a Zn concentration of 1000 μmol, the number of intergrowths continued to

increase, their sizes growing (200–300 µmol). At a Zn concentration of 2000 µmol, oxalate crystal intergrowths begin to break down (Figure 5c). In some areas of the mycelium, small crystals of second-generation katsarosite are observed (Figure 5d).

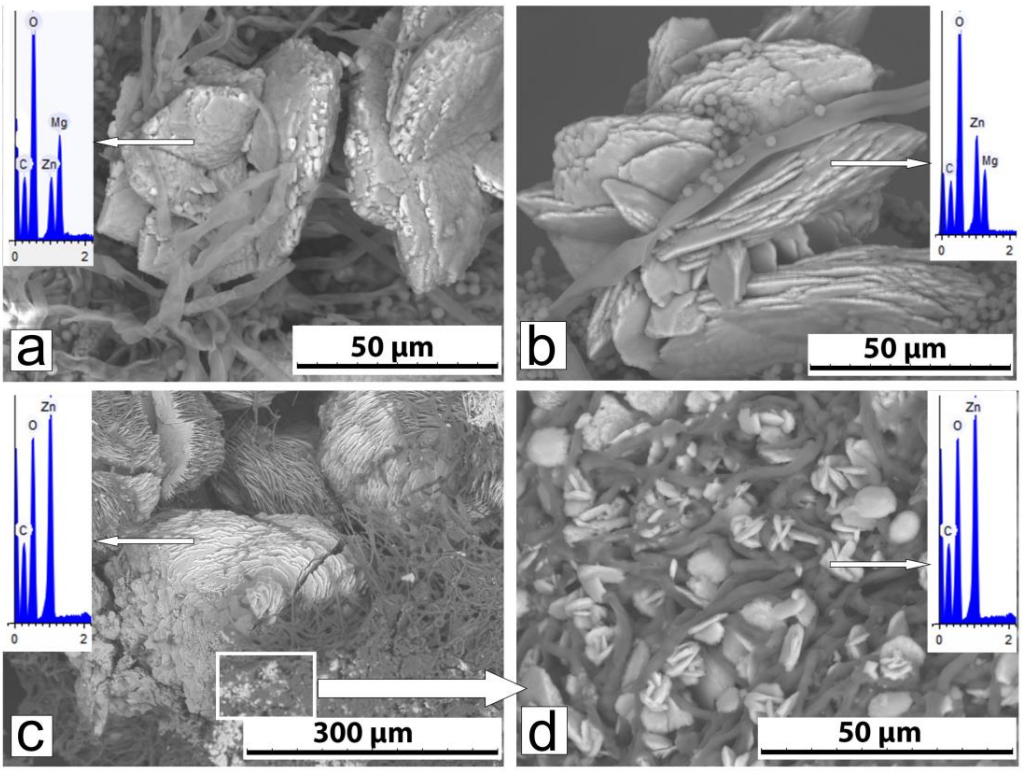

Figure 5. Intergrowths of Mg-Zn oxalate formed on the mycelium of *A. niger* at different Zn concentration: (**a**) Zn 250 µmol on the seventh day, (**b**) Zn 500 µmol on the twenty-eighth day, (**c**) Zn 2000 µmol on the twenty-eighth day, (**d**) fragment of this Figure c in which small plate crystals of second-generation katsarosite are visible. The arrow indicates the point on crystals at which the EDX measurement was performed.

Hopeite formation

According to the SEM and PXRD data, a zinc phosphate hopeite $Zn_3(PO_4)_2X4H_2O$ formed without fungal participation is present on the seventh day at all Zn concentrations, and at 2000 µmol, it is preserved on the fourteenth and twenty-first days (Figure 6a,b, Table 3). On the twenty-eighth day, hopeite crystals were not visible on the mycelium.

Large plate-shaped abiogenic hopeite crystals are characterized by rounded edges, which indicates their dissolution under the action of fungal metabolites. On the mycelium, very small crystals are grouped near and at some distance from abiogenic crystals. This crystal encrusts hyphae, resulting in the formation of tubular fungal structures (Figure 6c). PXRD, SEM, and EDX study of mycelial fragments showed that these are biogenic hopeite crystals (Figure 6d).

3.2.3. Phase Composition and Morphology of Crystals Formed Under Action of *P. chrysogenum*

As in the case of *A. niger*, in the absence of Zn, no oxalates and phosphates occurred on the *P. chrysogenum* mycelium. In the region of 2θ Cu = 9.2° (Figure 4b, X phase), the diffraction peak is also present in the XRD patterns of Zn-containing crystallization products.

Hopeite formation

According to PXRD, SEM, and EDX data, a lot of hopeite crystals are present on the mycelium at all Zn concentrations (Figure 4b, Table 4). Large needle-shaped and plate-shaped hopeite crystals that formed without the participation of the fungus at all Zn

concentrations are visible. These crystals had a smooth surface, with mycelium imprints and traces of dissolution formed under the action of fungal metabolites (Figure 3b). As the Zn concentration increased, they became more abundant. With the age of the cultures, the hopeite crystals undergo strong splitting, which leads to the formation of fan-shaped and spherulite-like structures (Figure 3c).

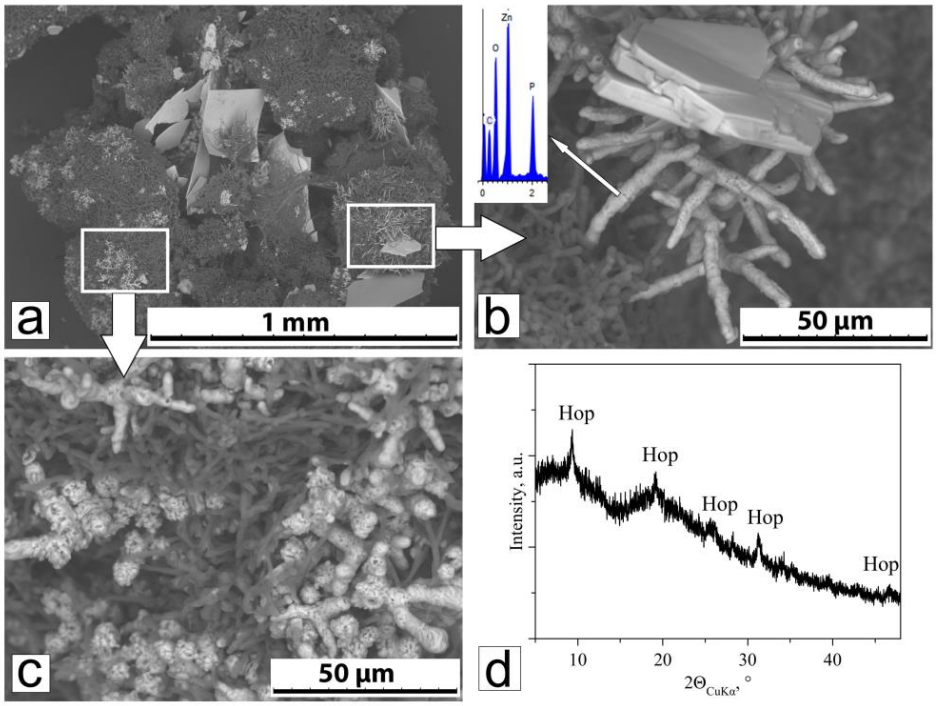

Figure 6. Crystals and intergrowth of zinc phosphate hopeite on the mycelium of *A. niger* in a liquid medium with Zn 2000 µmol on the fourteenth day: (**a**–**c**) SEM images of large plate-shaped abiogenic crystals with rounded edges and very small biogenic crystals encrust hyphae and form tubular fungal structures, (**d**) PXRD of tubular fungal structures.

Table 4. Phase composition of crystals formed on *P. chrysogenum* mycelium at different Zn concentration.

Days	Zn Concentration in Solution, µmol							
	250		500		1000		2000	
	Phase Composition	**pH**	**Phase Composition**	**pH**	**Phase Composition**	**pH**	**Phase Composition**	**pH**
7	Hop (ab)	7.0	Hop (ab)	7.0	Hop (ab)	6.0	No fungal growth	6.0
14		7.5		8.0	**Hop (bio)**, Hop (ab)	6.5	Hop (ab)	4.8
21		6.9		8.0	**Hop (bio)**, Hop (ab), (Zn0.5Mg0.5)Ox (α) > (Zn0.5Mg0.5)Ox (α) > Zn-MgOx (α)	7.0	**Hop (bio)**, Hop(ab) >> Kat	5.6
28	Hop(ab), Zn-MgOx (α) > (Zn0.5Mg0.5)Ox (α)	9.0	Hop (ab), (Zn0.5Mg0.5)Ox (α) > Zn-MgOx (α)	8.0		8.0	**Hop (bio)**, Hop(ab), Kat	6.3

Notes: Hop (ab)—abiogenic hopeite, **Hop (bio)**—biogenic hopeite, Zn-MgOx—Zn-containing Mg-oxalate, Kat—katsarosite, α—monoclinic oxalate modification.

At a Zn concentration of 1000 µmol, on the fourteenth day, very small crystals were found in some areas of the mycelium, which encrust the hyphae, resulting in the formation

of tubular fungal structures (Figure 7a,b). According to the morphology and to the EDX spectrum, these structures are formed by biogenic secondary hopeite, described above in the case of *A. niger* at 2000 µmol and at 14 days of growth.

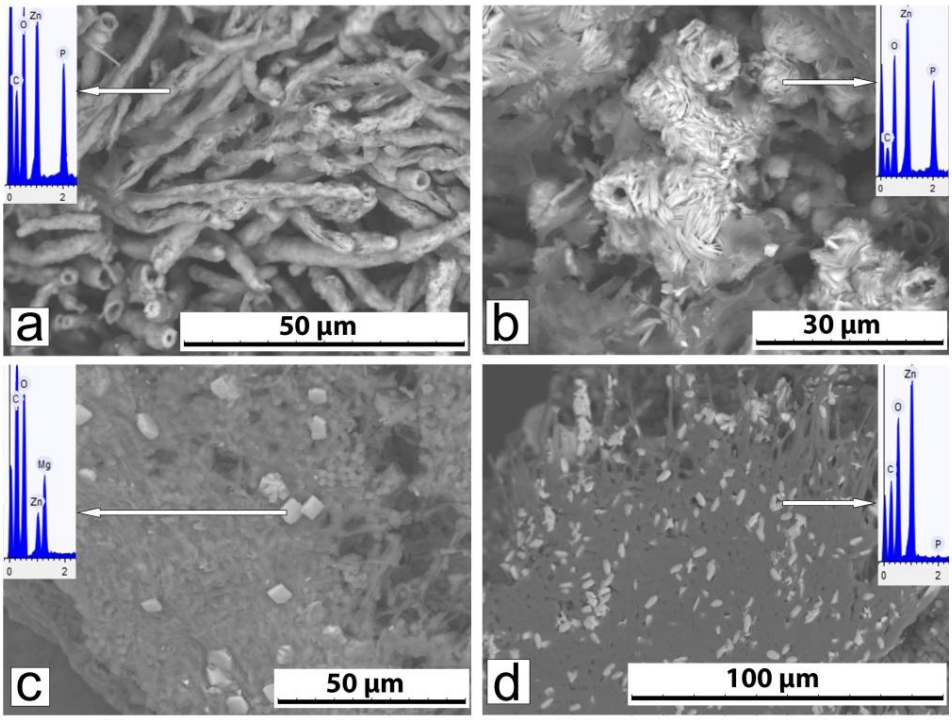

Figure 7. Crystals on the mycelium of *P. chrysogenum* with different Zn concentrations: (**a**,**b**) biogenic crystals, very small biogenic crystals, and tubular fungal structures of zinc phosphate hopeite at Zn 1000 µmol on the twenty-first and twenty-eighth day; (**c**,**d**) small crystals of Mg-Zn oxalates at 250 and 2000 Zn µmol on the twenty-eighth and twenty-first day, respectively. The arrow indicates the point on crystals at which the EDX measurement was performed.

On the twenty-first day, the mycelium was intensively encrusted with phosphate tubular fungal structures, 2–5 µm in diameter. On the twenty-eighth day, the composition of the crystallization products was similar as on the twenty-first day. The abundance of phosphate tubular fungal structures increased; it is clearly seen that these structures consist of individual lamellar crystals (Figure 7b).

At a Zn concentration of 2000 µmol, intensive formation of phosphate tubular fungal structures was observed on the twenty-first day. By the twenty-eighth day, the number of phosphate tubular fungal structures encrusting the mycelium increased. The fact that these crystals, like in the case of *A. niger*, were formed by hopeite was additionally confirmed via the PXRD.

Metal oxalates formation

Small Mg-Zn oxalate crystals were detected only using SEM and EDX (Figure 7c,d) at late stages of fungal culture growth (21 and 28 days of experiment), when oxalic acid accumulated in the medium (Table 2). The products of biogenic crystallization at the lowest Zn concentration (250 µmol) on the twenty-eighth day were represented by small (5–10 µm in size), single, short, prismatic (box-like), close-to-isometric crystals, present in very small quantities. EDX data (Figure 7c) and the presence of oxalic acid in the medium (Table 2) indicate that these are crystals of Mg-Zn oxalates (Mg/Zn = 1.05–2.05). At a Zn concentration of 500 µmol, on the twenty-eighth day, the contents of Mg and Zn become closer (Mg/Zn = 1.05–1.4). At a Zn concentration of 1000 µmol, on the twenty-first and twenty-eight days, Mg-Zn oxalates (Mg/Zn = 1.3 to 1.8) appeared in the mycelium along with phosphates.

At a Zn concentration of 2000 µmol, Zn oxalates katsarosite (without Mg) was detected on the twenty-first and twenty-eight days (Figure 7d). On the twenty-eighth day, the amount of katsarosite became sufficient to determine their PXRD (Figure 4b).

4. Discussion

4.1. Zinc Effect on the Growth and Metabolism of A. niger and P. chrysogenum

The results showed that the growth and metabolism of the fungi *A. niger* and *P. chrysogenum* were significantly dependent on the Zn concentration on the medium. Bioavailable Zn in concentrations of 192–432 µmol (at a total Zn concentration of 250–500 µmol Zn) acted as a physiologically essential element, activating the growth of fungal mycelium. The presence of two-phase growth (exponential and stationary phases) on the Zn-free medium and on media with low Zn concentrations (250–500 µmol) is associated with glucose consumption by fungi [56]. During active growth (exponential phase), the medium contains sufficient glucose, when the glucose concentration decreases, the growth rate slows down and the growth curve reaches a stationary phase. With an increase in concentrations to 639–1626 µmol (1000–2000 µmol total Zn), Zn acted as a toxic heavy metal, inhibiting fungal growth. Due to the slow growth of the mycelium, glucose is consumed more slowly, and the culture and exponential phase are longer. The presence of zinc in such concentrations in the natural environment is classified as potentially hazardous [38].

P was in excess and remained in the medium mainly in bound forms in the culture liquid of both types of fungi throughout the entire experiment. Accordingly, the fungi did not experience phosphorus starvation.

Both species of fungi produce low-molecular organic acids, but the content of oxalic acid, without which the formation of oxalates is impossible, in the culture liquid of *A. niger* was significantly higher (by 10 times or more, Tables 1 and 2). The same can be said about the content of citric acid, which, as was shown earlier, is not phase-forming, but has a significant effect on the phase composition of crystallization products and the morphology of the resulting crystals [52,59]. The intensity of oxalic acid production increased in both species under the influence of Zn, especially in *A. niger* (Table 1), which is in good agreement with the literature data [18,60]. In addition, Zn suppressed the production of citric acid by *A. niger*, probably due to a higher carbon requirement for oxalate biosynthesis.

The composition of metabolic products, primarily organic acids production, controlled the pH of the cultural liquid. In the culture of *A. niger*, with an increase in the concentrations of free oxalic and citric acids, pH decreased to 2 (Figure 2a, Table 1). However, at a Zn concentration of 2000 µmol (on the fourteenth and twenty-eighth days), it was less acidic and was close to neutral (5–6). Unlike *A. niger*, in the culture liquid of *P. chrysogenum*, alkalization of the medium occurred (the pH value increased to 9). This was facilitated by the content of oxalic acid in the culture of *P. chrysogenum* being an order of magnitude lower and completely bound into insoluble salts. In addition, the alkalization of the medium was probably facilitated by the hydrolysis of urea with the formation of NH_4^+ as a result of enzyme urease activity produced by *P. chrysogenum*. Urease activity also determines the decrease in *P. chrysogenum* biomass on the twenty-eighth day: NH_4^+ accumulating as a result of urea hydrolysis promotes mycelium lysis [61]. Slight acidification of the medium occurred (up to 4.8) at a Zn content 1000 and 2000 µmol, which can be explained by the fact that high Zn concentrations can inhibit urease and thus prevent alkalization of the medium.

4.2. Zinc Concentration Effect of on Fungal Biomineralization

The pH values of the culture liquid, along with the concentration of phase-forming ions, significantly affected the interrelated processes of dissolution and crystallization occurring under the fungal activity. As shown above, in the Czapek–Dox nutrient medium

at pH = 6.0, without fungi, tetrahydrate zinc phosphate hopeite is formed immediately after autoclaving (Figure 3).

In the Zn-containing acidic medium of the *A. niger* culture liquid, crystals of this primary abiogenic zinc phosphate are intensively dissolved. We record them only at the beginning of the experiment (on the seventh day) at close to neutral medium with a Zn content of 2000 mmol (on the fourteenth and twenty-first days) (Figure 6b, Table 3). Small crystals of biogenic hopeite are visible near the rapidly dissolving crystals of abiogenic hopeite, which encrust hyphae and form tubular fungal structures (Figure 6b,c).

In the alkaline Zn-containing medium of the *P. chrysogenum* culture liquid, abiogenic hopeite is almost insoluble. The diffraction peaks of hopeite (Figure 4b) are associated mainly with abiogenic phosphate. Dissolution of abiogenic (formed at the beginning of the experiment) and the parallel formation of secondary biogenic hopeite are observed only at high zinc contents in a close to neutral or slightly acidic medium (at a Zn content of 1000 mmol (on the fourteenth and twenty-first days); at a Zn content of 2000 μmol (on the twenty-first and twenty-eighth days)). Thus, our studies have shown that zinc phosphate hopeite is formed under the action of fungi in slightly alkaline and slightly acidic environments (close to neutral in pH). In an acidic medium (below 5), it dissolves too quickly, and in an alkaline medium (above 7), it almost does not dissolve, which leads to an insufficient content of free Zn in the solution.

Unlike phosphate, oxalate crystallization occurs with the participation under activity of both fungal species at all Zn concentrations in a wide range of pH (from 2 to 9.0). As a result, solid solutions of katsarosite–glushinskite of the isodimorphic series with the general formula $(Zn,Mg)C_2O_4 \cdot 2H_2O$ are formed. The difference in the oxalate-producing ability of fungi is manifested in the fact that under the activity of *A. niger,* the required amount of oxalic acid is already accumulated in the medium on the seventh day of the experiment, and under the activity of *P. chrysogenum*, not earlier than after 20 days of the experiment (at high Zn concentrations). At the highest Zn concentration (2000 μmol), in the culture of both fungal species, zinc oxalate $ZnC_2O_4 \cdot 2H_2O$ (monoclinic α-modification) is formed (an analog of the biomineral katsarosite found in lichens), belonging to the monoclinic α-modification. On the mycelium of *A. niger* grown at a Zn content of 1000 and 500 μmol, there are oxalate grains with predominance of both Zn and Mg coming from the nutrient medium, which allows us to speak about the formation of Mg-containing katsarosite and its Zn-containing magnesium analog. Moreover, as the Zn decreases, the magnesium analog of the katsarosite gradually begins to predominate. With a Zn concentration of 250 μmol, on the mycelium only, the Zn-containing magnesium analog of katsarosite forms, as well as orthorhombic β-modification of magnesium oxalate (analog of the mineral glushinskite), which allows us to speak about the isodimorphic transition of katsarosite–glushinskite in the range between 500 and 250 μmol Zn in the medium.

On the mycelium of *P. chrysogenum,* the crystallization conditions are more favorable for the incorporation of Mg into katsarosite. This effect, like in the case of the incorporation of Mg into lindbergite [52], cannot be explained only by the presence of citric acid in the medium (there is more of it in the culture of *A. niger*). When the Zn content in the medium is less than 2000 μmol, oxalates with a predominance of Zn are not formed. Monoclinic α-modification is represented by solid solutions with close Zn and Mg content $(Zn0.5Mg0.5)C_2O_4 \cdot 2H_2O$, which cannot be attributed to either katsarosite or its magnesium structural analog, and the Zn-containing magnesium analog of katsarosite. The katsarosite–glushinskite transition probably occurs when the Zn content in the medium is less than 250 μmol.

Under the action of both species of fungi, stabilization of the structure of katsarosite (monoclinic α-modification) is observed: on the mycelium of *A. niger,* up to the ratio

Mg/Zn = 5, and on the mycelium of *P. chrysogenum*, up to Mg/Zn = 2, which can be associated with the stabilizing effect of Zn. A similar effect was observed upon the entry of Mg into the monoclinic manganese oxalate lindbergite, in which the stabilizing effect of Mn cations manifested itself up to the ratio Mg/Mn = 1.5 [52].

The above-described patterns of phase formation in the Czapek–Dox medium at different Zn concentrations under the effect of fungi are one example of microbially induced biomineralization [62]. However, at concentrations of 1000 and 2000 mmol, Zn acts as a toxic element that can lead to partial death of the microorganisms and, accordingly, to the destruction of cells. Therefore, at high zinc concentrations, we (strictly speaking) should already talk about mixed biomineralization, since crystals formed inside the cell under its direct control can also enter into the mycelium in small quantities. Controlled biomineralization, in contrast to induced biomineralization, is often associated with non-classical two-stage nucleation/crystallization processes [63–65], which are characterized by a lower free energy compared to the corresponding classical mechanisms.

4.3. The Prospects for Using the A. niger and P. chrysogenum in Biotechnologies for Zn Detoxifying

Both species of fungi have the ability to convert Zn into insoluble forms, reducing its bioavailability and toxicity. Zn detoxification by oxalic acid accumulated in the medium occurred by its inclusion in insoluble oxalates in a wide pH range (2.5–9.0).

The intensity of oxalate mineralization in the *A. niger* culture was incomparably greater than that in *P. chrysogenum*, which is a consequence of the difference in the intensity of oxalic acid production activity by these fungi described above. In the culture liquid of *A. niger*, as the concentration of Zn in the medium increased, the amount of bound oxalic acid increased, and free oxalic acid decreased, which clearly indicates the role of oxalate biomineralization in the detoxification of Zn excess. On the other hand, the intensive production of organic acids by *A. niger* leads to the dissolution of hopeite (both abiogenic and biogenic) and, consequently, to an increase in the concentration of free Zn in the medium and an increase in its toxic effect. However, in the studied system, a very high content of oxalic acid in the culture liquid of *A. niger* led to rapid binding of free Zn. As a result, oxalates were formed in significantly greater quantities than phosphates, and the detoxification process prevailed. On the mycelium of *P. chrysogenum*, zinc oxalates were formed in incomparably smaller quantities than in *A. niger*.

Obviously, the intensity of oxalate formation in *P. chrysogenum* was insufficient for the effective detoxification of excess amounts of Zn, at its initially high concentrations in the medium. Nevertheless, at high Zn concentrations 1000 and 2000 μmol, *P. chrysogenum* grew no less actively than *A. niger*, and the mycelium of *P. chrysogenum* was abundantly encrusted with secondary hopeite. The intensive formation of biogenic hopeite also confirms that by the end of the experiment (28 days), up to 50% of $H_2PO_4^-$, HPO_4^{2-}, and PO_4^{3-} were in a bound form.

The obtained data showed that *A. niger* and *P. chrysogenum* can be used for Zn environmental detoxification. With the participation of both types of fungi, oxalates and phosphates are formed in Zn-containing media. The ratio of fungal oxalates and phosphates is directly dependent on the acid-reducing capacity of the fungi: under the influence of *A. niger*, oxalates are predominantly formed, and under the influence of *P. chrysogenum*, phosphates are predominantly formed.

5. Conclusions

This in vitro study of the metabolism effect of *A. niger* and *P. chrysogenum* on phase formation in Zn-containing media showed the promise of using the fungi in biotechnologies

for detoxifying heavy metals. It was demonstrated that not only oxalate but also phosphate biomineralization can be applied. It was found that the ratio of formed fungal oxalates and phosphates is directly dependent on the acid-production activity of the fungi, which allows it to be controlled by selecting the appropriate strains. The application of phosphate biomineralization seems promising in the case of severe pollution. To create a near-neutral medium favorable for the formation of phosphates, it is advisable to use soil fungi non-producing or weakly producing organic acids (for example, *P. chrysogenum*).

Author Contributions: Conceptualization, K.V.S., M.S.Z., O.V.F.-K. and D.Y.V.; methodology, K.V.S., M.S.Z., O.V.F.-K. and A.V.K.; investigation, K.V.S., M.S.Z., O.V.F.-K., E.V.B. and A.V.K.; writing—original draft preparation, K.V.S. and M.S.Z.; writing—review and editing, O.V.F.-K. and D.Y.V.; visualization, M.S.Z.; supervision, O.V.F.-K. and D.Y.V. All authors have read and agreed to the published version of the manuscript.

Funding: The study of fungal metabolism was carried out within the framework and with funding from the research project «Development of profiling-metabolomic methods for the study of biological objects» (124020100140-7) of the Komarov Botanical Institute of the Russian Academy of Sciences.

Data Availability Statement: No new data were created or analyzed in this study. Data sharing is not applicable to this article.

Conflicts of Interest: Anatoliy V. Korneev and Elena V. Bakhvalova were employed by "ECROSKHIM" Ltd. The remaining authors declare that the research was conducted in the absence of any commercial or financial relationships that could be construed as a potential conflict of interest.

References

1. Mukhopadhyay, M.; Noronha, S.B.; Suraishkumar, G.K. A review on experimental studies of biosorption of heavy metals by Aspergillus niger. *Can. J. Chem. Eng.* **2011**, *89*, 889–900. [CrossRef]
2. Tian, D.; Jiang, Z.; Jiang, L.; Su, M.; Feng, Z.; Zhang, L.; Wang, S.; Li, Z.; Hu, S. A new insight into lead (II) tolerance of environmental fungi based on a study of Aspergillus niger and Penicillium oxalicum. *Environ. Microbiol.* **2019**, *21*, 471–479. [CrossRef] [PubMed]
3. Chandran, S.C.; Shijith, K.V.; Vipin, K.V.; Augusthy, A.R. Study on heavy metals toxicity biomarkers in Aspergillus niger. *Int. J. Adv. Pharm. Biol. Chem.* **2014**, *3*, 458–464.
4. Ashruta, G.A.; Nanoty, V.; Bhalekar, U. Biosorption of heavy metals from aqueous solution using bacterial EPS. *Int. J. Life Sci.* **2014**, *2*, 373–377.
5. Bhattacharya, A.; Gupta, A.; Kaur, A.; Malik, D. Simultaneous bioremediation of phenol and Cr (VI) from tannery wastewater using bacterial consortium. *Int. J. Appl. Sci. Biotechnol.* **2015**, *3*, 50–55. [CrossRef]
6. Zhao, R.; Wang, B.; Cai, Q.T. Bioremediation of hexavalent chromium pollution by Sporosarcinasaromensis m52 isolated from offshore sediments in Xiamen, China. *Biomed. Environ. Sci.* **2016**, *29*, 127–136. [CrossRef]
7. Goher, M.E.; El-Monem, A.M.A.; Abdel-Satar, A.M.; Ali, M.H.; Hussian, A.-E.M.; Napiórkowska-Krzebietke, A. Biosorption of some toxic metals from aqueous solution using non-living algal cells of Chlorella vulgaris. *J. Elem.* **2016**, *21*, 703–714. [CrossRef]
8. Marzan, L.W.; Hossain, M.; Mina, S.A.; Akter, Y.; Chowdhury, A.M.M.A. Isolation and biochemical characterization of heavy-metal resistant bacteria from tannery effluent in Chittagong city, Bangladesh: Bioremediation viewpoint. *Egypt. J. Aquat. Res.* **2017**, *43*, 65–74. [CrossRef]
9. Saranya, K.; Sundaramanickam, A.; Shekhar, S.; Swaminathan, S.; Balasubramanian, T. Bioremediation of mercury by vibrio fluvialis screened from industrial effluents. *BioMed Res. Int.* **2017**, *2017*, 6509648. [CrossRef]
10. Nayan, A.K.; Panda, S.S.; Basu, A.; Dhal, N.K. Enhancement of toxic Cr(VI), Fe, and other heavy metals phytoremediation by the synergistic combination of native Bacillus cereus strain and veltiveria of phytoremediation. *J. Phytoremediation* **2018**, *20*, 682–691. [CrossRef]
11. Abioye, O.P.; Oyewole, O.A.; Oyeleke, S.B.; Adeyemi, M.O.; Orukotan, A.A. Biosorption of lead, chromium and cadmium in tannery effluent using indigenous microorganisms. *Braz. J. Biol. Sci.* **2018**, *5*, 25–32. [CrossRef]
12. Rehan, M.; Alsohim, A.S. Bioremediation of Heavy Metals. In *Environmental Chemistry and Recent Pollution Control Approaches*; Saldarriaga-Noreña, H., Murillo-Tovar, M.A., Farooq, R., Dongre, R., Riaz, S., Eds.; IntechOpen: London, UK, 2019. [CrossRef]
13. Dhankhar, R.; Hooda, A. Fungal biosorption–an alternative to meet the challenges of heavy metal pollution in aqueous solutions. *Environ. Technol.* **2011**, *32*, 467–491. [CrossRef]

14. Achal, V.; Pan, X.; Zhang, D. Remediation of copper-contaminated soil by Kocuria flava CR1, based on microbially induced calcite precipitation. *Ecol. Eng.* **2011**, *37*, 1601–1605. [CrossRef]
15. Girbal, J.; Prada, J.L.; Rocabayera, R.; Argemi, M. Dating of Biodeposits of Oxalates at the Arc De Berà in Tarragona, Spain. *Radiocarbon* **2001**, *43*, 637–645. [CrossRef]
16. Gadd, G.M. Geomycology: Biogeochemical transformations of rocks, minerals, metals and radionuclides by fungi, bioweathering and bioremediation. *Mycol. Res.* **2007**, *111*, 3–49. [CrossRef]
17. Purvis, O.W.; Pawlik-Skowrońska, B.; Cressey, G.; Jones, G.C.; Kearsley, A.; Spratt, J. Mineral phases and element composition of the copper hyperaccumulator lichen Lecanora polytropa. *Mineral. Mag.* **2008**, *72*, 607–616. [CrossRef]
18. Sazanova, K.; Osmolovskaya, N.; Schiparev, S.; Yakkonen, K.; Kuchaeva, L.; Vlasov, D. Organic Acids Induce Tolerance to Zinc- and Copper-Exposed Fungi Under Various Growth Conditions. *Curr. Microbiol.* **2015**, *70*, 520–527. [CrossRef]
19. Sazanova, K.V.; Frank-Kamenetskaya, O.V.; Vlasov, D.Y.; Zelenskaya, M.S.; Vlasov, A.D.; Rusakov, A.V.; Petrova, M.A. Carbonate and Oxalate Crystallization by Interaction of Calcite Marble with Bacillus subtilis and Bacillus subtilis–Aspergillus niger Association. *Crystals* **2020**, *10*, 756. [CrossRef]
20. Zhao, J.; Csetenyi, L.; Gadd, G.M. Fungal-induced $CaCO_3$ and $SrCO_3$ precipitation: A potential strategy for bioprotection of concrete. *Sci. Total Environ.* **2022**, *816*, 151501. [CrossRef]
21. Cotter-Howells, J.; Caporn, S. Remediation of contaminated land by formation of heavy metal phosphates. *Appl. Geochem.* **1996**, *11*, 335–342. [CrossRef]
22. Basta, N.; McGowen, S.L. Evaluation of Chemical Immobilization Treatments for Reducing Heavy Metal Transport in a Smelter-Contaminated Soil. *Environ. Pollut.* **2004**, *127*, 73–82. [CrossRef] [PubMed]
23. Yiwen, Z.; Maxwell, S.L.; Runting, R.K.; Carrasco, L.R. Environmental destruction not avoided with the Sustainable Development Goals. *Nat. Sustain.* **2020**, *3*, 795–798. [CrossRef]
24. Bajda, T.; Rogowska, M.; Pawłowska, R.A. Synthesis and solubility of hopeite $Zn_3(PO_4)_2 \cdot 4H_2O$. *Mineralogia* **2023**, *54*, 78–81. [CrossRef]
25. Fomina, M.; Alexander, I.J.; Hillier, S.; Gadd, G.M. Zinc Phosphate and Pyromorphite Solubilization by Soil Plant-Symbiotic Fungi. *Geomicrobiol. J.* **2004**, *21*, 351–366. [CrossRef]
26. Doilom, M.; Guo, J.-W.; Phookamsak, R.; Mortimer, P.E.; Karunarathna, S.C.; Dong, W.; Liao, C.-F.; Yan, K.; Dhandevi, P.; Suwannarach, N.; et al. Screening of Phosphate-Solubilizing Fungi From Air and Soil in Yunnan, China: Four Novel Species in Aspergillus, Gongronella, Penicillium, and Talaromyces. *Front. Microbiol.* **2020**, *11*, 585215. [CrossRef]
27. Suyamud, B.; Ferrier, J.; Csetenyi, L.; Inthorn, D.; Gadd, G.M. Biotransformation of struvite by Aspergillus niger: Phosphate release and magnesium biomineralization as glushinskite. *Environ. Microbiol.* **2020**, *22*, 1588–1602. [CrossRef]
28. Kang, X.; Csetenyi, L.; Gao, X.; Gadd, G.M. Solubilization of struvite and biorecovery of cerium by Aspergillus niger. *Appl. Microbiol. Biotechnol.* **2022**, *106*, 821–833. [CrossRef]
29. Bhalla, K.; Qu, X.; Kretschmer, M.; Kronstad, J.W. The phosphate language of fungi. *Trends Microbiol.* **2022**, *30*, 338–349. [CrossRef]
30. Leng, Y.; Colston, R.; Soares, A. Understanding the biochemical characteristics of struvite bio-mineralising microorganisms and their future in nutrient recovery. *Chemosphere* **2020**, *247*, 125799. [CrossRef]
31. Leng, Y.; Soares, A. The mechanisms of struvite biomineralization in municipal wastewater. *Sci. Total Environ.* **2021**, *799*, 149261. [CrossRef]
32. Soares, A.; Veesam, M.; Simoes, F.; Wood, E.; Parsons, S.A.; Stephenson, T. Bio-Struvite: A New Route to Recover Phosphorus from Wastewater. *Clean—Soil Air Water* **2014**, *42*, 994–997. [CrossRef]
33. Ennever, J.; Summers, F.E. Calcification by Candida albicans. *J. Bacteriol.* **1975**, *122*, 1391–1393. [CrossRef] [PubMed]
34. Rhee, Y.J.; Hillier, S.; Gadd, G.M. Lead Transformation to Pyromorphite by Fungi. *Curr. Biol.* **2012**, *22*, 237–241. [CrossRef] [PubMed]
35. Xu, X.; Hao, R.; Xu, H.; Lu, A. Removal mechanism of Pb(II) by Penicillium polonicum: Immobilization, adsorption, and bioaccumulation. *Sci. Rep.* **2020**, *10*, 9079. [CrossRef]
36. Liang, X.; Hillier, S.; Pendlowski, H. Uranium phosphate biomineralization by fungi. *Environ. Microbiol.* **2015**, *17*, 2064–2075. [CrossRef]
37. Sazanova, K.V.; Zelenskaya, M.S.; Izatulina, A.R.; Korneev, A.V.; Vlasov, D.Y.; Frank-Kamenetskaya, O.V. Carbonate and Oxalate Crystallization Effected by the Metabolism of Fungi and Bacteria in Various Trophic Conditions: The Case of Penicillium chrysogenum and Penicillium chrysogenum with Bacillus subtilis. *Crystals* **2023**, *13*, 94. [CrossRef]
38. Grassi, C.; Cecchi, S.; Baldi, A.; Zanchi, C.A.; Orlandini, S.; Pardini, A.; Napoli, M. Crop suitability assessment in remediation of Zn contaminated soil. *Chemosphere* **2020**, *246*, 125706. [CrossRef]
39. Van, H.-T.; Hoang, V.H.; Nga, L.T.; Nguyen, Q.V.Q. Effects of Zn pollution on soil: Pollution sources, impacts and solutions. *Results Surf. Interfaces* **2024**, *17*, 100360. [CrossRef]
40. Barreto, M.S.C.; Elzinga, E.J.; Rouff, A.A.; Siebecker, M.G.; Sparks, D.L.; Alleoni, L.R.F. Zinc speciation in highly weathered tropical soils affected by large scale vegetable production. *Sci. Total Environ.* **2024**, *916*, 170223. [CrossRef]

41. Rahman, S.H.; Khanam, D.; Adyel, T.M.; Islam, M.S.; Ahsan, M.A.; Akbor, M.A. Assessment of Heavy Metal Contamination of Agricultural Soil around Dhaka Export Processing Zone (DEPZ), Bangladesh: Implication of Seasonal Variation and Indices. *Appl. Sci.* **2012**, *2*, 584–601. [CrossRef]
42. Salnikova, E.V.; Burtseva, T.I.; Skalnaya, M.G.; Skalny, A.V.; Tinkov, A.A. Copper and zinc levels in soil, water, wheat, and hair of inhabitants of three areas of the Orenburg region, Russia. *Environ. Res.* **2018**, *166*, 158–166. [CrossRef] [PubMed]
43. Hussain, S.; Khan, M.; Sheikh, T.M.M.; Mumtaz, M.Z.; Chohan, T.A.; Shamim, S.; Liu, Y. Zinc Essentiality, Toxicity, and Its Bacterial Bioremediation: A Comprehensive Insight. *Front. Microbiol.* **2023**, *17*, 1133733. [CrossRef] [PubMed]
44. Siddiquee, S.; Rovina, K.; Al Azad, S. Heavy Metal Contaminants Removal from Wastewater Using the Potential Filamentous Fungi Biomass: A Review. *J. Microb. Biochem. Technol.* **2015**, *7*, 384–393. [CrossRef]
45. Sutjaritvorakul, T.; Gadd, G.M.; Whalley, A.; Sihanonth, P. Zinc Oxalate Crystal Formation by Aspergillus nomius. *Geomicrobiology* **2015**, *33*, 289–293. [CrossRef]
46. Sayer, J.A.; Gadd, G.M. Binding of cobalt and zinc by organic acids and culture filtrates of Aspergillus niger grown in the absence or presence of insoluble cobalt or zinc phosphate. *Mycol. Res.* **2001**, *105*, 1261–1267. [CrossRef]
47. Frank-Kamenetskaya, O.; Vlasov, D. Crystallization induced by fungi and bacteria. *Acta Cryst.* **2025**, *B81 Pt 1*, 1–10. [CrossRef]
48. Giester, G.; Rieck, B.; Lengauer, C.L.; Kolitsch, U.; Nasdala, L. Katsarosite Zn(C2O4)·2H2O, a new Humboldtine-Group Mineral from the Lavrion Mining District, Greece. *Mineral. Pet.* **2023**, *117*, 259–267. [CrossRef]
49. Zelenskaya, M.S.; Izatulina, A.R.; Frank-Kamenetskaya, O.V.; Vlasov, D.Y. Iron Oxalate Humboldtine Crystallization by Fungus *Aspergillus Niger*. *Cryst.* **2021**, *11*, 1591. [CrossRef]
50. Atencio, D.; Coutinho, J.; Graeser, S.; Matioli, P.; Lindbergite, F.L. A New Mn Oxalate Dihydrate from Boca Rica Mine, Galiléia, Minas Gerais, Brazil, and Other Occurences. *Am. Mineral.* **2004**, *89*, 1087–1091. [CrossRef]
51. Baran, E. Review: Natural oxalates and their analogous synthetic complexes. *J. Coord. Chem.* **2014**, *67*, 23–24. [CrossRef]
52. Korneev, A.V.; Izatulina, A.R.; Kuz'mina, M.A.; Frank-Kamenetskaya, O.V. Solid Solutions of Lindbergite–Glushinskite Series: Synthesis, Ionic Substitutions, Phase Transformation and Crystal Morphology. *Int. J. Mol. Sci.* **2022**, *23*, 14734. [CrossRef] [PubMed]
53. Sazanova, K.V.; Zelenskaya, M.S.; Korneev, A.V.; Vlasov, D.Y. Extracellular Zn Detoxication by *Penicillium chrysogenum* and *Aspergillus niger*. *Mycol. Phytopathol.* **2023**, *57*, 425–434b. [CrossRef]
54. Herschke, L.; Enkelmann, V.; Lieberwirth, I.; Wegner, G. The role of hydrogen bonding in the crystal structures of zinc phosphate hydrates. *Chem.—Eur. J.* **2004**, *10*, 2795–2803. [CrossRef] [PubMed]
55. Etesami, H.; Jeong, B.R.; Glick, B.R. Contribution of Arbuscular Mycorrhizal Fungi, Phosphate-Solubilizing Bacteria, and Silicon to P Uptake by Plant. *Front. Plant Sci.* **2021**, *12*, 699618. [CrossRef]
56. Sazanova, K.V.; Vlasov, D.Y.; Osmolovskay, N.G.; Schiparev, S.M.; Rusakov, A.V. Significance and regulation of acids production by rock-inhabited fungi. In *Biogenic—Abiogenic Interactions in Natural and Anthropogenic Systems. Lecture Notes in Earth System Sciences*; Frank-Kamenetskaya, O., Panova, E., Vlasov, D., Eds.; Springer: Cham, Switzerland, 2016; pp. 379–392.
57. Sturm, E.V.; Frank-Kamenetskaya, O.V.; Vlasov, D.Y.; Zelenskaya, M.S.; Sazanova, K.V.; Rusakov, A.V.; Kniep, R. Crystallization of calcium oxalate hydrates by interaction of calcite marble with fungus Aspergillus niger. *Am. Mineral.* **2015**, *100*, 2559–2565. [CrossRef]
58. Krake, S.; Conzelmann, C.; Heuer, S. Production of chitosan from Aspergillus niger and quantitative evaluation of the process using adapted analytical tools. *Biotechnol. Bioprocess* **2024**, *E29*, 942–954. [CrossRef]
59. Rusakov, A.; Kuz'mina, M.; Frank-Kamenetskaya, O. Biofilm Medium Chemistry and Calcium Oxalate Morphogenesis. *Molecules* **2021**, *26*, 5030. [CrossRef]
60. Fomina, M.; Hillier, S.; Charnock, J.M.; Melville, K.; Alexander, I.J.; Gadd, G.M. Role of oxalic acid overexcretion in transformations of toxic metal minerals by Beauveriacaledonica. *Appl. Environ. Microbiol.* **2005**, *71*, 371–381. [CrossRef]
61. Hess, C.D.; Lu, W.; Rabinowitz, D.J.; Botstein, D. Ammonium toxicity and potassium limitation in yeast. *PLoS Biol.* **2006**, *4*, 2012–2023. [CrossRef]
62. Berenjian, A.; Seifan, M. *Mineral Formation by Microorganisms. Concepts and Applications*; Berenjian, A., Seifan, M., Eds.; Springer: Cham, Switzerland, 2022; 387p.
63. Colfen, H.; Mesocrystals, A.M. *Nonclassical Crystallization*; John Wiley & Sons: Hoboken, NJ, USA, 2008; 288p.
64. L'vov, P.E.; Umantsev, A.R. Two-Step Mechanism of Macromolecular Nucleation and Crystallization: Field Theory and Simulations. *Cryst. Growth Des.* **2021**, *21*, 366–382. [CrossRef]
65. Askhabov, A.M. Problem of building units in crystal growth and genesis of non-classical concepts of crystal formation. *Vestn. Geosci.* **2022**, *11*, 20–24. [CrossRef]